CHAPTER 8
OPTIMIZATION OF USSP DURATION FOR ENHANCED CORROSION RESISTANCE

8.1 Introduction

This chapter presents optimization of the duration of the ultrasonic shot peening (USSP) for enhancement in corrosion resistance of this alloy. USSP was performed for different durations of 5, 10, 15, 20, 25, 30 seconds with steel balls of 3 mm diameter at an amplitude of 80 μm and the samples are designated as USSP 5, USSP 10, USSP 15, USSP 20, USSP 25 and USSP 30, respectively. The un-USSP treated and different USSP treated samples were subjected to potentiodynamic polarization and electrochemical impedance spectroscopy. Among the specimens USSP treated from 5 to 30 seconds, the one USSP treated for 15 seconds (USSP 15) was found to exhibit highest corrosion potential (E_{corr}) and lowest corrosion current density (i_{corr}). Corrosion products were characterized by Scanning Electron Microscopy (SEM) and X-ray Photoelectron Spectroscopy (XPS). Scanning Kelvin Probe Force Microscopy (SKPFM) was used to measure the surface free potential. The corrosion resistance of the USSP 15 sample was found to be the highest due to combined effect of surface nanostructure of the matrix, homogeneity and refinement of the second phase precipitates. USSP15 specimen showed higher corrosion resistance than to that of the un-USSP condition.

8.2 Scanning Kelvin Probe Force Microcopy

Fig. 8.1 shows surface Volta potential of the un-USSP and USSP 15 samples examined by in-situ AFM. There is difference in surface potential of the Al matrix and the surrounding intermetallic precipitates. From the line scan, it may be seen that Volta potential difference is positive at some places whereas it is negative at other places.

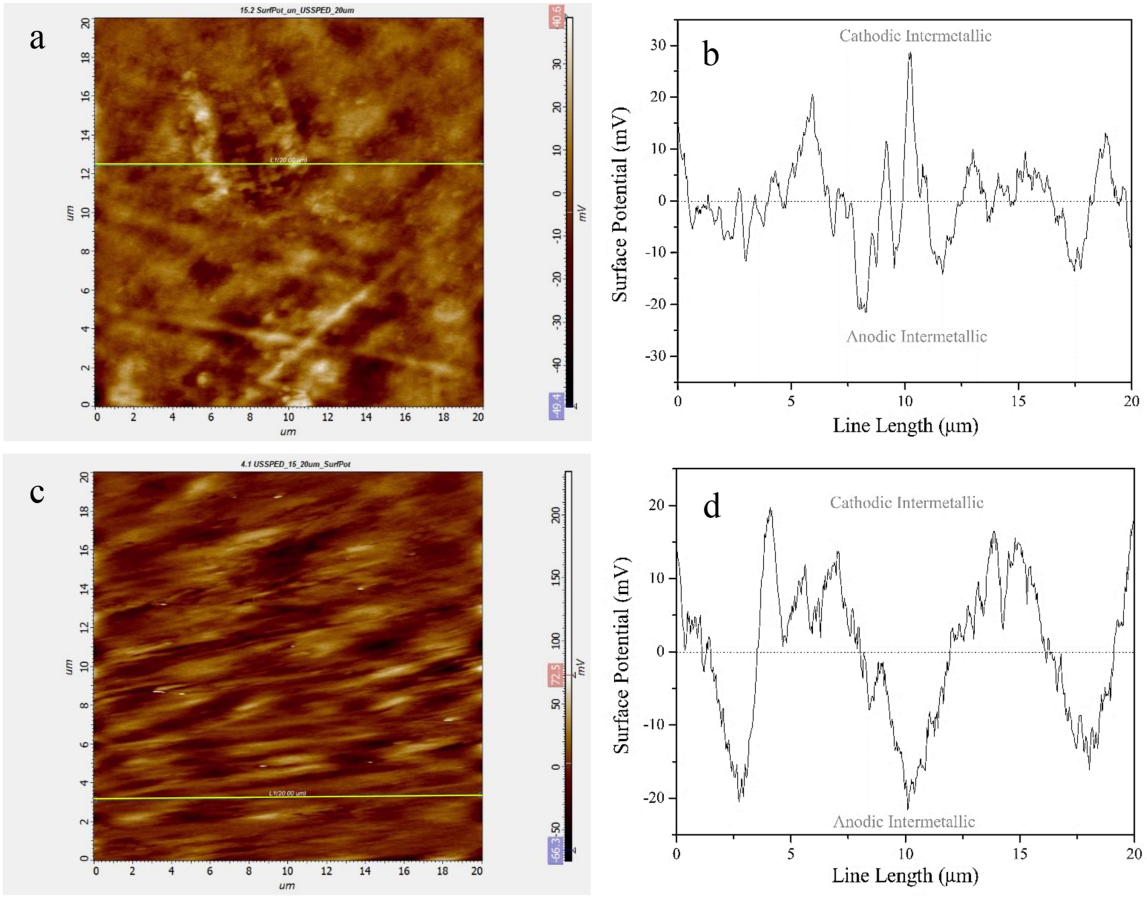

FIGURE 8.1: Volta potential map (a, c) and linear distribution of potential (b, d) for un-USSP and USSP 15 samples respectively.

In the un-USSP condition, the brighter area represents intermetallics with higher potential. The intermetallic showing positive Volta difference Fig. 8.1b is cathodic in nature with respect to the matrix having +28 mV to +20 mV potential difference. Mainly

these are Fe and Cu based second phase particles as reported earlier [167]. The anodic intermetallics are negative in nature with potential difference of -21 mV to -14 mV. This is due to the presence of Mg rich phases such as $MgZn_2$ and Mg_2Si [167]. For the USSP 15 sample the positive Volta potential difference lied in the range of +19 mV to +12 mV corresponding to Al matrix (Fig. 8.1d). Here the potential difference was less as compared to that of the un-USSP sample, showing stronger galvanic coupling between the matrix and the intermetallics in the un-USSP condition as compared to that in the USSP 15. On the other hand, there was very less effect on negative side of the Volta potential from -21 mV to -16 mV for the USSP 15 condition.

8.3 Corrosion Behavior

8.3.1 Potentiodynamic Polarization

Potentiodynamic polarization of the un-USSP and the different USSP treated samples was carried out in 3.5 wt.% NaCl solution following stabilization of the potential for 30 minutes. It is evident from the potentiodynamic plots in Fig. 8.2 that the samples USSP treated for more than 10 seconds show better corrosion resistance as compared with that of the un-USSP as revealed by decrease in the anodic and cathodic current density. In the anodic region of the polarization curves there is continuous increase in the corrosion current density without any tendency of passivation for the un-USSP, USSP 5 and USSP 10, whereas there are distinct passive regions for the USSP 15, USSP 20, USSP 25 and

USSP 30 specimens, however, the degree of passivation is different for the different conditions. It is highest for the USSP 15, followed by USSP 30, USSP 25 and USSP 20 in decreasing order. The passive films break down at particular potentials characterized as pitting potential (E_{pit}), the values of E_{pit} are presented in Table 8.1. Pitting occurs due to localized damage of the oxide film by Cl^- ions. The resistance of the oxide films on the different samples may be seen from the difference between E_{pit} and E_{corr}, which is highest for the USSP 15. The increase in corrosion current of the USSP 15 to USSP 30 is due to breakdown of passive film which can be seen from Fig. 8.2.

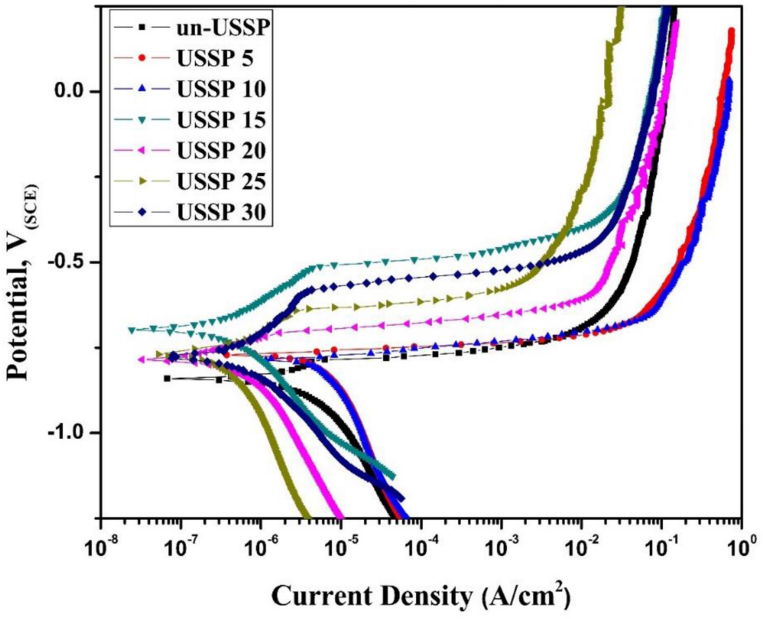

FIGURE 8.2: Potentiodynamic polarization curves in 3.5 wt% NaCl solution, after 30 minutes of their exposure.

The sudden increase in current density of the un-USSP, USSP 5 and USSP 10 is due to breakage of the native thin layer of the passive oxide film during anodic scanning. On the other hand, the USSP 15 and the other specimens USSP treated for longer durations show passivation phenomena and the USSP 15 shows nobler passive region with lower

current density. It may be seen from Fig. 8.2 that above E_{pit}, all the specimens exhibit limiting current density due to deposition of corrosion products which control the mass transfer at the interface of the specimen and solution. The limiting current density (i_{limit}) of the un-USSP treated, USSP 5 and USSP 10 are around 26.75, 83.86 and 103.53 μA/cm^2 respectively at -0.750 V. However, as the USSP duration is increased, its value decreases and reaches lowest for the USSP 25. As the duration of USSP increased, the roughness also increased and the process of corrosion was accelerated.

The electrochemical parameters such as corrosion current density (i_{corr}) and E_{corr} calculated by fitting the potentiodynamic curves in the Tafel region are shown in Table 8.1. The corrosion rate was calculated using the Platt equation.

$$Corrosionrate(\mu m/year) = \frac{3.27 \times 10^{-3} \times i_{corr} \times W_e}{d} \tag{8.1}$$

where the factor 3.27×10^{-3} includes the Faraday constant and the metric and time conversion factors, W_e represents the equivalent weight of Al alloy (9.98 g/mol), i_{corr} is the measured corrosion current density (μA/cm^2), and d is the density of the corroding element (2.81 g/cm^3). Corrosion rate of the un-USSP sample as recorded in Table 8.1, is found to be 44.19 μm/year whereas it is reduced to 20.06 μm/year for the USSP 15. The corrosion rate increases abruptly for the specimens treated initially up to 10 seconds, however, as the treatment time is increased up to 15 seconds its value is considerably reduced. Beyond this period of the USSP treatment, corrosion rate is increased again.

For the USSP 15 specimen, the value of E_{corr} shifted towards the nobler potential compared to that of the un-USSP and those of the other USSP treated samples. The other

TABLE 8.1: Electrochemical parameters of the un-USSP and USSP treated 7075 aluminium alloy in 3.5 wt% NaCl solution, after 30 minutes of their exposure.

Treatment condition	**E_{corr} (V_{SCE})**	**i_{corr} $\mu A/cm^2$**	**E_{pit} (V_{SCE})**	**E_{corr}-E_{pit} (V_{SCE})**	**Corrosion rate (μm/year)**
un-USSP	-0.839	1.269	-0.790	-0.049	44.19
USSP 5	-0.770	2.99	-0.759	-0.011	102.61
USSP 10	-0.785	5.13	-0.778	-0.007	176.02
USSP 15	-0.695	0.564	-0.517	-0.178	20.06
USSP 20	-0.786	0.68	-0.707	-0.079	26.67
USSP 25	-0.772	0.78	-0.642	-0.130	30.73
USSP 30	-0.778	1.07	-0.596	-0.182	38.10

USSP treated specimens exhibited E_{corr} between -0.770 to -0.785 V whereas the un-USSP treated exhibited -0.839 V which is more active than the USSP treated 15 (-0.695 V). This result suggests that the USSP treated 15 specimen forms protective and passive film on the surface in 3.5 wt.% NaCl solution. The E_{pit} and E_{corr} for the USSP 5 and USSP 10 are almost identical which reveals that these specimens are more active for pit formation due to USSP treatment. The most positive value of corrosion potential and lowest value of i_{corr} is shown by the USSP 15 sample reflecting lower dissolution rate and best corrosion resistance amongst all the tested specimens.

8.3.2 Electrochemical Impedance Studies

In order to have the interfacial information at the metal/solution interface in the aggressive environment, EIS was carried out in 3.5wt% NaCl solution for the different durations of exposure. Prior to EIS, samples were kept in 3.5 wt.% NaCl solution for stabilization of the potential. The Nyquist plots for the durations of exposure of 24 h and 360 h are shown in Fig. 8.3a and Fig. 8.3d respectively. It may be seen that Nyquist plots for all

the specimens are similar in shape but differ in diameter for the different durations of exposure. As the exposure period was increased up to 360 h (Fig. 8.3d), the diameter of the Nyquist plots at lower and higher frequencies was reduced. This suggests that all the specimens exhibited deterioration in corrosion properties from longer duration of exposure. However, the USSP 15 shows larger diameter of the Nyquist plots at lower frequency where the tail is longer compared to those of the other specimens. In the range of higher to middle frequency, the diameter of Nyquist plots even for the 360 h of exposure is larger in size than those of the other specimens.

The log modulus-frequency Bode plots for the tested specimens are shown in Figs. 8.3b and 8.3e. It can be seen from Fig. 8.3b that after 24 h of exposure in 3.5 wt.%NaCl solution, the USSP 15 specimen shows highest impedance compared with the others at the lowest studied frequency of 0.01 Hz. The impedance decreased for the USSP 10 and is less for the un-USSP specimen. The impedance is maximum for the USSP 15 sample, however, beyond this it tends to decrease. As the period of exposure increased up to 360 h in 3.5 wt.%NaCl, the impedance gradually decreased for all the specimens (Fig. 8.3e). The phase-frequency Bode plots of the specimens exposed in 3.5 wt.% NaCl solution are shown in Fig. 8.3c & Fig. 8.3f. From this it can be seen that the USSP 15 specimen exhibits two inflections (two-time constants) at different frequencies, one in the range of middle frequency which indicates capacitive properties of the passive film formed during the process of corrosion while the other one in the range of lower frequency indicating occurrence of reaction at metal/solution interface.

EIS spectra of the un-USSP and different USSP treated specimens were fitted with

suitable electrical circuit shown in Fig. 8.4. Such type of circuit has already been established by Domı´nguez-Crespo et al. for Al metal surface exposed in 3.5% NaCl solution [168]. In this model R_p is polarization resistance, R_u is solution resistance between solution and the reference electrode, Q is constant phase element (CPE) parameter,W_d is Warburg diffusion coefficient and alpha (α) is CPE exponent. The analyzed data using the equivalent electrical circuit are recorded in Table 8.2.

It is evident from the data of the Table 8.2 that polarization resistance (R_p) for un-USSP samples which is considerably lower than USSP 15 samples exposed for 24 h. This trend is the same for 360 h exposed samples. Beyond 15 seconds of USSP the polarization resistance of samples gradually have decreasing trend both for 24 h and 360 h exposure. The value of Y_o which indicate that porosity of passive film is lowest for USSP 15 sample in comparision to un-USSP and samples treated for other duration. USSP 15 sample exhibit the lowest warburg diffusion coefficient in comparision to un-USSP and USSP treated samples. All the factors suggest that USSP 15 sample develops a protective passive film on its surface.

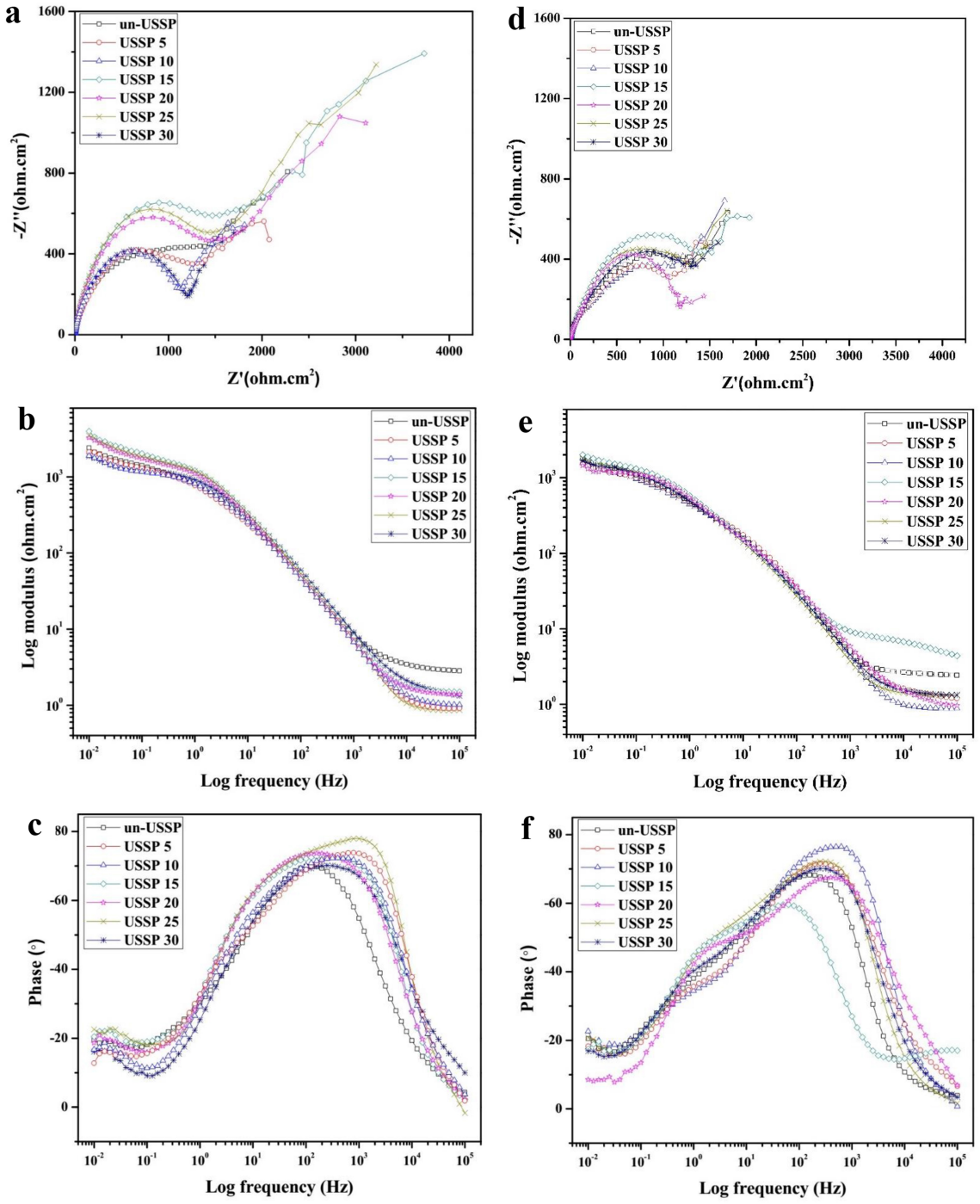

FIGURE 8.3: EIS plots of the un-USSP and different USSP treated samples in 3.5 wt% NaCl solution recorded at their respective open circuit potentials for immersion duration of (a-c) 24 h and (d-f) 360 h respectively.

TABLE 8.2: EIS parameters of the un-USSP and USSP treated samples for different exposure durations in 3.5 wt% NaCl solution recorded at their respective open circuit potentials.

Treatment Condition	**Immersion time (h)**	**Electrochemical parameters**					
		$\mathbf{R}_u(\Omega\mathbf{cm}^2)$	$\mathbf{R}_p(\Omega\mathbf{cm}^2)$	$\mathbf{Y}_0$ $(\Omega^{-1}\mathbf{cm}^{-2}\mathbf{Sn})(\mathbf{x10}^{-5})$	α	$\mathbf{W}_d(\mathbf{Ss}^{1/2}\mathbf{x}\ \mathbf{10}^{-3})$	**Chi-sqaure(x 10^{-3})**
un-USSP	24	2.828	994.5	10.91	0.80	2.645	5.171
	360	2.275	723.4	17.4	0.78	3.021	16.31
USSP 5	24	0.774	959.1	11.3	0.80	3.097	17.55
	360	0.750	646.6	19.4	0.77	3.571	18.11
USSP 10	24	0.928	946.4	11.6	0.80	4.259	5.013
	360	0.806	402.0	39.4	0.60	5.540	23.46
USSP 15	24	1.368	1470	7.79	0.85	1.70	4.840
	360	5.209	1403	8.59	0.84	1.737	13.46
USSP 20	24	1.328	1349	8.66	0.82	1.953	2.567
	360	0.842	1163	9.72	0.81	2.037	11.25
USSP 25	24	0.764	1297	8.99	0.81	2.151	10.52
	360	1.174	962.0	11.5	0.79	2.691	16.67
USSP 30	24	1.297	1091	9.71	0.81	2.20	1.906
	360	1.195	855.0	16.1	0.78	2.830	17.29

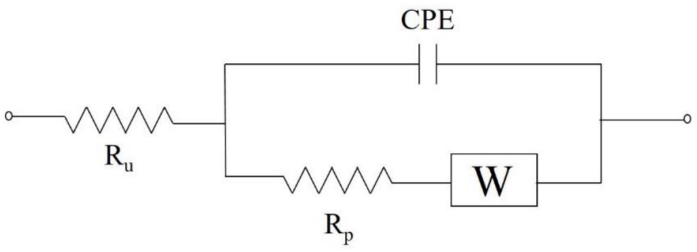

FIGURE 8.4: Equivalent electrical circuit

8.3.3 Potentiodynamic behavior after 360 hours of exposure

Corrosion characteristics of the oxide/passive film formed on surface of the un-USSP and USSP treated samples was examined by potentiodynamic studies after 360 hours of exposure in 3.5 wt.% NaCl solution. The potentiodynamic plots are shown in Fig. 8.5 and the different calculated corrosion parameters are presented in Table 8.3. The anodic reaction for all the conditions started from their respective E_{corr} and passive regions formed at 1.5 $\sim$ 2.0 μA/cm^2 up to -0.730 V. The trans-passive region is observed around -0.750 V up to -0.300 V at 0.64 μA/cm^2 to 7.11 μA/cm^2 anodic current density except for the un-USSP and USSP 5 specimens which was found to be up to -0.467 V, thereafter E_{pit} started. The un-USSP specimen exhibited i_{lim} at 189.0 μA/cm^2 at -0.361 V due to deposition/formation of large amount of porous corrosion products. After careful analysis of the extracted electrochemical data in Table 8.3 it can be inferred that the E_{pit} of the USSP 15 is noble (-0.281 V) and i_{corr} is 2-7 times lower than those of the other specimens. It reflects the excellent adherent and protective nature of the passive film formed on its surface. On comparison of the potentiodynamic results after 30 min and 360 h of exposure, it is found that at the longer duration of exposure all the specimens show higher corrosion,

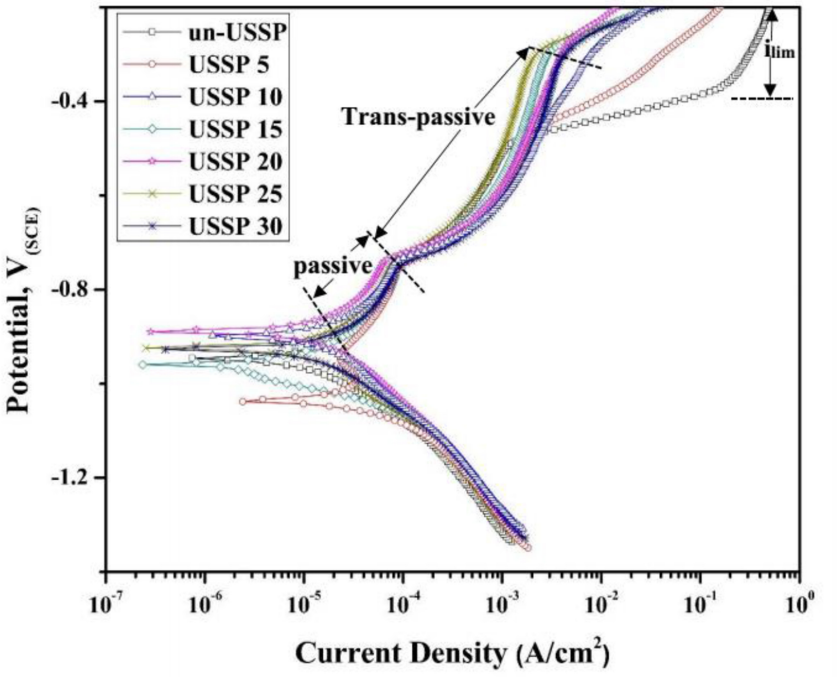

FIGURE 8.5: Potentiodynamic polarization curves of the un-USSP and USSP treated specimens after 360 h of exposure in 3.5 wt.% NaCl solution

TABLE 8.3: Electrochemical parameter of the un-USSP and USSP treated specimens after 360 h of exposure in 3.5 wt.% NaCl solution.

Treatment Condition	**E_{corr} (V_{SCE})**	**i_{corr} ($\mu A/cm^2$)**	**E_{pit} (V_{SCE})**	**Corrosion Rate (μm/Year)**
un-USSP	-0.947	27.20	-0.467	917.44
USSP 5	-1.030	31.60	-0.467	1065.78
USSP 10	-0.900	40.70	-0.294	1373.37
USSP 15	-0.959	6.260	-0.281	211.09
USSP 20	-0.889	12.10	-0.298	407.41
USSP 25	-0.924	17.60	-0.298	592.58
USSP 30	-0.928	18.10	-0.298	612.14

but among them the USSP 15 is the best from the point of view of corrosion resistance in 3.5 wt.%NaCl solution.

8.3.4 X-ray Photoelectron Spectroscopy

XPS characterization was carried out for the specimens before and after 360 h of EIS in 3.5 wt.%NaCl. High resolution XPS curve fitted spectra are presented in Fig. 8.6. In the fitted spectra of the un-USSP and USSP 15 specimens before exposure to 3.5 wt.% NaCl XPS Al2p spectrum are shown in Fig. 8.6a and 8.6c, respectively and two peaks have appeared.

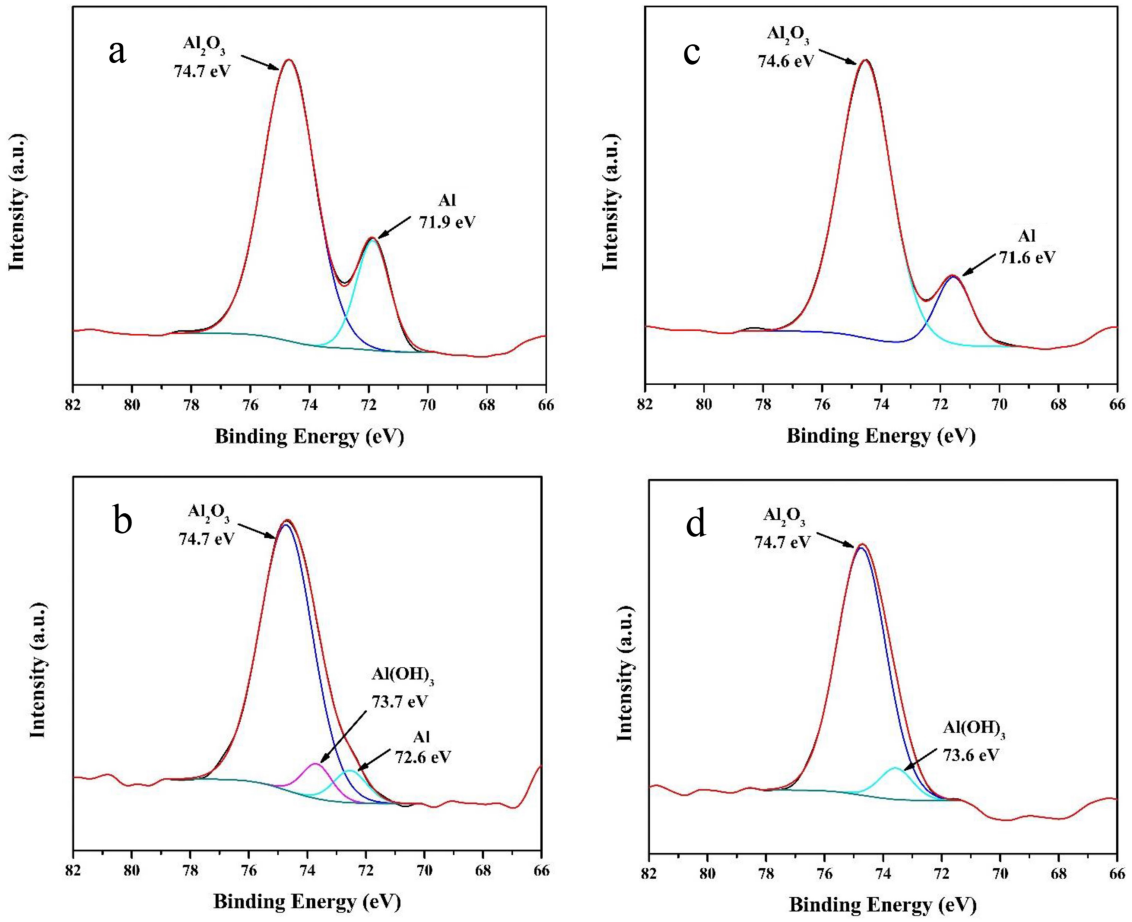

FIGURE 8.6: XPS Al2p spectrum of different samples: (a) un-USSP, (b) un-USSP+360h of exposure, (c) USSP 15 and (d) USSP 15+360h of exposure.

The first peak of higher intensity from Al_2O_3 may be seen to appear at 74.7 eV and 74.6 eV whereas the second peak from the matrix appeared at 71.9 eV and 71.6 eV for the

un-USSP and USSP 15 specimens respectively. After the exposure of 360 h in the 3.5 wt% NaCl an additional peak of $Al(OH)_3$ along with the peaks of Al_2O_3 and Al matrix was also observed in the un-USSP condition. On the other hand, for the USSP 15 condition only two peaks, one of Al_2O_3 and the other of$Al(OH)_3$ were observed and peak of Al matrix was absent. The appearance of $Al(OH)_3$ peak after exposure suggests change in chemical state of the surface.

8.4 Stress Corrosion Behavior

AA7075 is susceptible to stress corrosion cracking because of precipitate free zones (PFZ). Since there is an improvement of corrosion resistance after USSP, it is intuitive that the SCC resistance of this alloy may improve due to USSP. In order to study the effect of USSP treatment on stress corrosion sensitivity, slow strain rate tests (SSRT) were carried out for the specimens in air and also in NaCl solution. Since, the USSP 15 showed the best corrosion resistance this was selected to study the SCC behavior of the alloy. Fig. 8.7 shows the stress vs strain curves of the un-USSP and USSP specimens after the SSRT tests.The time to failure are indicated in Fig. 8.8. The stress vs strain plots in Fig. 8.7 are for both 3.5 wt% NaCl solution and air for the samples in un-USSP and USSP treated conditions. The values of the yield strength (YS), ultimate tensile strength (UTS) and total elongation (e_t) calculated from the stress-strain plot is shown in Table 8.4

The un-USSP specimen in air exhibited YS 358 MPa and UTS 517 MPa with total elongation of 5.98%. Whereas, the un-USSP sample in NaCl solution showed reduction in YS, UTS and e_t. The USSP treated specimen tested in air, showed higher YS of 394

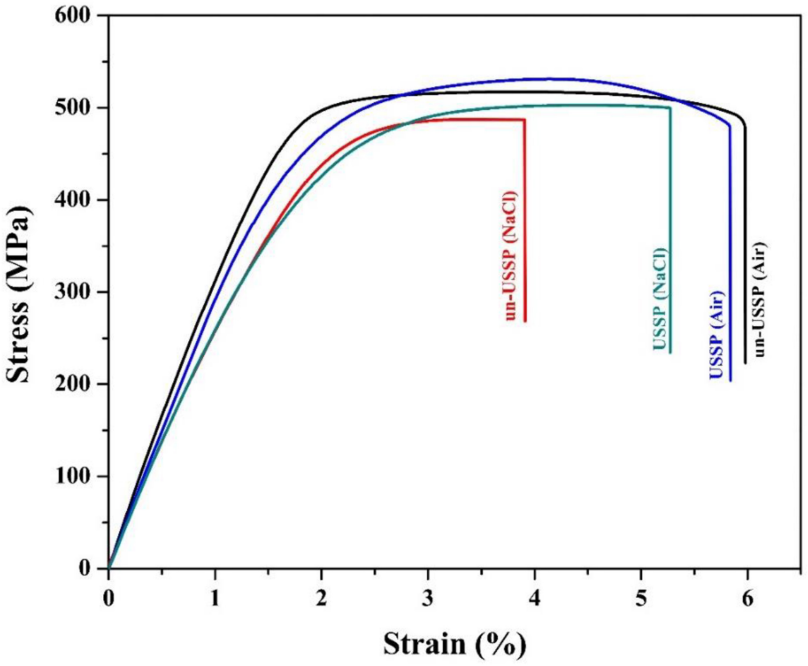

FIGURE 8.7: Stress-Strain curves of un-USSP and USSP specimens in Air and 3.5 wt.% NaCl solution at slow strain rate of 10^{-6} s^{-1}.

TABLE 8.4: Mechanical properties calculated from SSRT tests.

Treatment Condition	YS (MPa)	UTS (MPa)	e_t (%)
un-USSP (Air)	385	517	5.98
un-USSP (NaCl)	353	487	3.91
USSP (Air)	394	531	5.84
USSP (NaCl)	356	503	5.27

MPa, UTS of 531 MPa as compared to that of the un-USSP condition, however, the total elongation was found to decrease. The USSP specimen tested in NaCl solution also showed lower values as to those of the samples tested in air. Additionally, from Fig. 8.8 it is clear that the time to failure was found to decrease in the sample exposed to NaCl solution as to that of the sample tested in air and for the USSP treated sample the time to failure was found to increase as compared to that of the un-USSP condition. The above results indicate that USSP treatment sufficiently enhanced the stress corrosion resistance of the AA7075. The stress corrosion sensitive coefficient can be calculated using the

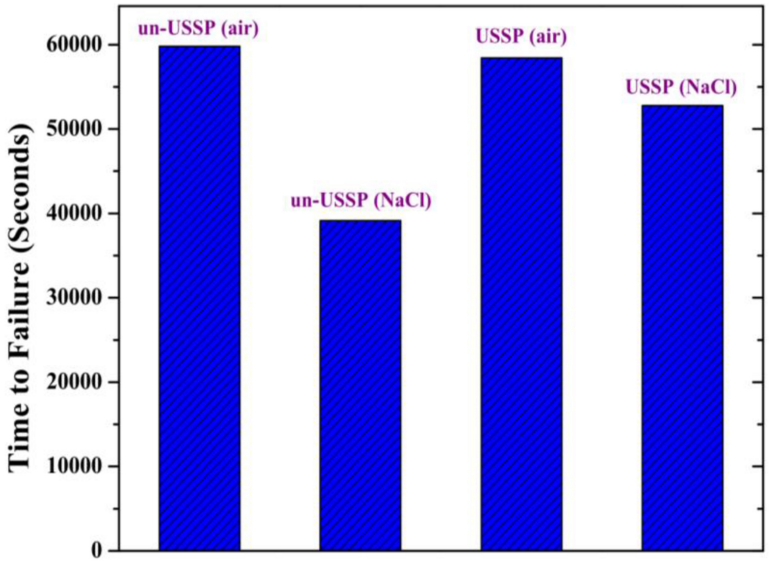

FIGURE 8.8: Time to failure of SSRT tests for the un-USSP and USSP conditions.

following formula:

$$I_{SSRT} = 1 - \frac{\sigma_S(1+\delta_s)}{\sigma_A(1+\delta_A)} \tag{8.2}$$

where, I_{SSRT} is stress corrosion sensitive coefficient; σ_S and σ_A are the ultimate tensile strength in 3.5 wt.% NaCl solution and air; δ_S and δ_A are the total elongation in 3.5 wt.% NaCl solution and air. Using the above formula the stress corrosion sensitive coefficient was deduced and it was found to be 33.7% and 13.2% for the un-USSP and USSP conditions. A high I_{SSRT} value indicates a high susceptibility to stress corrosion cracking (SCC), that is to say the specimens can be more easily corroded. Thus, the USSP treated specimens were less sensitive than the un-USSP in the 3.5 wt.% NaCl solution at a strain rate of 1X10^{-6} s^{-1}. The results indicate that USSP remarkably improves the stress corrosion resistance of the AA7075.

8.5 Discussion

Potentiodynamic polarization curves clearly show enhanced corrosion resistance of the samples USSP treated for 15-30 seconds. i_{corr} and E_{corr} values are the measure of corrosion resistance. The USSP 15 sample showed lowest i_{corr} and nobler E_{corr} which clearly indicate its higher corrosion resistance. The USSP 20, USSP 25 and USSP 30 samples also showed better corrosive properties than that of the un-USSP. Anodic portion of polarization curves of the samples show continuous increase in current density with some tendency of passivation for the USSP 15, USSP 20, USSP 25 and USSP 30 samples. The range of passive plateau is highest for the USSP 15 followed by the USSP 30, USSP 25 and USSP 20. This suggests that an anodic potential shift of passive plateau of about -0.178 V is due to the stability of the passive film which is attributed to presence of nanocrystalline surface layer [78]. Increase in current density is due to initiation of localized corrosion. The rapid increase in current density after passivation is designated as pitting potential (E_{pit}).The USSP 15 sample shows passivation up to -0.517 V from its OCP (open circuit potential) before the breakdown, whereas passive region was not present in the case of USSP 5 and USSP 10 samples. It was due to rapid increase in the roughness from the USSP treatment which hindered the formation of passive layer.

The SEM micrographs of the un-USSP and USSP 15 sample after potentiodynamic polarization (Fig. 8.9) shows that there was pitting tendency over entire surface of the specimen. Severe pitting was observed on the surface of the un-USSP sample as compared with that of the USSP 15. It is clear from EDS analysis of the pits (indicated by circle) that pits are enriched in Mg, Zn and Si suggesting that pitting has occurred mainly close to the

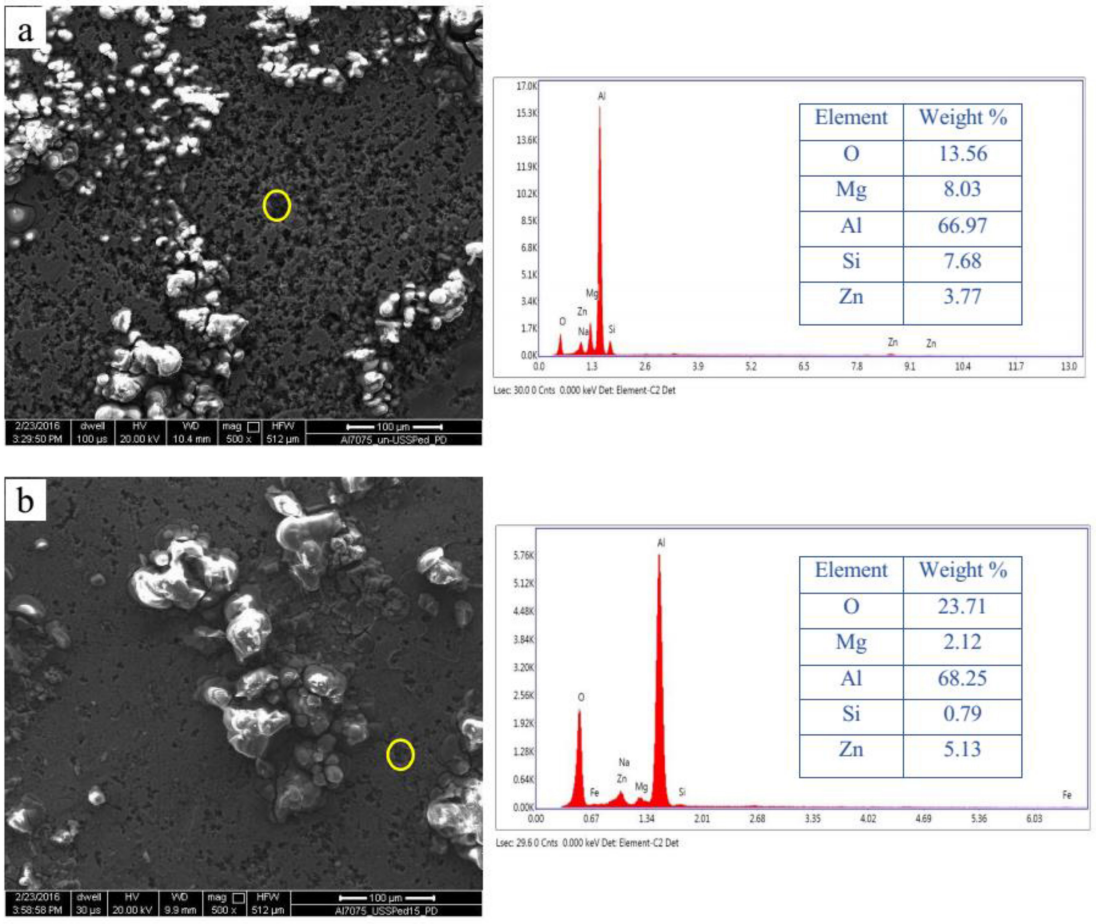

FIGURE 8.9: Morphology and the corresponding EDS of the AA7075 after potentiodynamic polarization in 3.5 wt% NaCl solution (a) un-USSP and (b) USSP 15.

second phase particles or the precipitates. In the un-USSP condition it is due to the coarse intermetallic particles, mainly along the grain boundaries which cause localized corrosion and breakdown immediately above the E_{corr}. Therefore, the presence of intermetallic particles like Mg_2Si and coarse $MgZn_2$ precipitates at the grain boundaries leads to higher corrosion rate in the un-USSP condition [73]. For the USSP 15 sample the severity of pitting was rather less and confined to isolated regions which could be defects, craters or second phase particles. These particles act either anodic or cathodic with respect to matrix and cause localized corrosion [169].This is due to galvanic coupling between the

precipitates and the matrix because of the potential difference between them. In the USSP 15 condition the second phase particles could have undergone dissolution therefore there were very less active sites on the surface for corrosion to occur. It was also confirmed by the SKPFM studies (Fig. 8.1) that the volta potential difference was less for the USSP 15 as compared to that of the un-USSP, indicating a stronger galvanic coupling for the un-USSP condition. Therefore, USSP 15 sample exhibited better corrosion resistance than that of the un-USSP [170]. The anodic intermetallics have the same volta potential (-21 mV) in both un-USSP and USSP 15 condition, whereas there is some difference in volta potential for the cathodic intermetallics (+28 mV & +19 mV). Hence, the corrosion resistance of the 7075 aluminium alloy can be attributed to difference in volta potential of the cathodic intermetallics.

It can be explained from the schematic shown in Fig. 8.10 that in case of the un-USSP samples the coarse second phase particles cause localized corrosion and lead to large size pits, whereas in the USSP treated samples the refinement/dissolution of the second phase particles restricts the tendency of localized corrosion. The area surrounding the particles shows galvanic coupling which is more in the un-USSP condition due to large volta potential difference and it is found to be less in the USSP 15 condition. Due to this there was formation of a very thin and stable passive layer on the surface of the USSP 15 sample. Hence, the enhanced corrosion resistance of the USSP 15 sample may be attributed to nanostructured surface layer and finer second phase precipitates.

In the Nyquist plot, there was formation of two depressed semi-circle loops for the

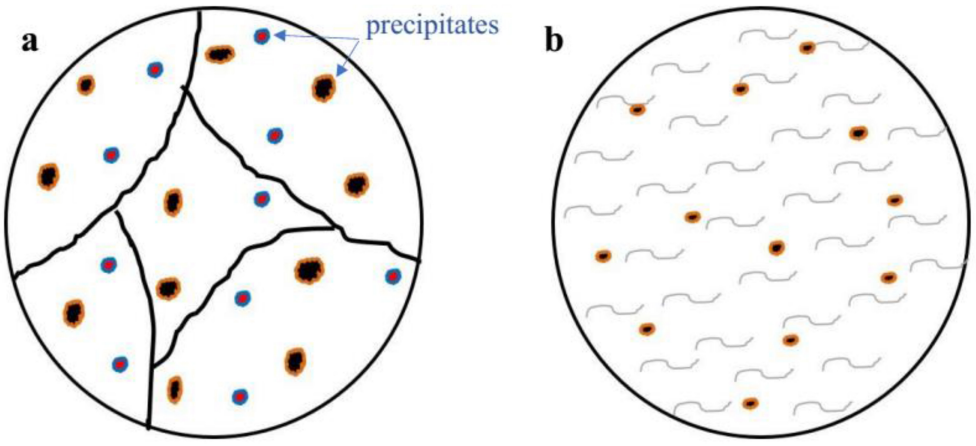

FIGURE 8.10: Schematic showing surface morphology of (a) un-USSP and (b) USSP treated specimen.

both 24 h as well as 360 h of exposures. It can be seen from Fig. 8.3a and d that the un-USSP treated and all the USSP treated samples exhibited a depressed semi-circular loop in the complex impedance plane with the center under the real axis (Z' real), which is a typical behavior of solid metal electrodes showing frequency dispersion in the impedance data [171]. Also, all the specimens show a tail in the region of lower frequency which can be attributed to thin oxide film or diffusion control process [172, 173]. The semi-circular loop at higher frequency is due to the resistance caused by oxide film formed on metal/solution interface and capacitance of the charge transfer process while at lower frequency a straight line reveals the Warburg impedance which shows characteristic features of diffusion within the Al alloy specimen [174, 175]. The $MgZn_2$ precipitates on the surface of the alloy 7075 are susceptible to Cl^- ions and undergo dissolution in the un-USSP condition whereas these precipitates get fragmented in the samples USSP treated for higher durations. Initially, for the USSP treated samples the formation of passive film is enhanced when it reacts with NaCl. On much longer exposure of 360 h, the diameter

of the loop is decreased due to formation of thick oxide layer which caused decrement in the polarization resistance (R_p). These results clearly show that the passive film formed on the USSP treated samples is not effective for longer duration of exposure, however, it is much better as compared to that formed on the un-USSP specimen.

The log modulus-frequency plots show that the impedance was highest for the USSP 15 sample at the frequency of 0.01 Hz for the both, 24 h as well as 360 h of exposures in 3.5 wt.%NaCl solution and thus further strengthens the observed high corrosion resistance of USSP 15. The highest impedance of the USSP 15 sample is attributed to formation of highly effective passive film on the surface, being more resistant to penetration of Cl^- ions, than the films formed on the other USSP treated samples. However, its resistance is reduced on long exposure of 360 h (Fig. 8.3e). With further increase in the USSP duration the impedance was found to decrease, suggesting that as the USSP duration is increased the surface becomes more susceptible to Cl^- ions attack. It was lowest for the USSP 10 sample, which may be attributed to abrupt increase in surface roughness interfering the formation of protective passive layer to reduce the corrosion resistance. On longer duration of exposure of 360 h the impedance was found to decrease for all the conditions, suggesting that oxide layer is porous in nature and the initially formed passive layer is thin which becomes less stable and prone to ingress of Cl^- ions, hence impedance is decreased. In phase-frequency plots broad phase angle peak is observed for 24 h of immersion, whereas the maxima is narrower and gets shifted towards lower phase after 360 h of exposure (Fig. 8.3f). The shifting of maxima towards lower phase indicates deposition of corrosion products on the surface. In the electrochemical equivalent circuit,

W_d is due to the diffusion process taking place, indicating porous and inhomogeneous nature of the passive/oxide film. The diffusion coefficient was found to increase on 360 h of exposure for the each tested condition. It reflects less effectiveness of the oxide film formed in checking the flow of aggressive ions towards the substrate [176].

Three regions were distinguished from the polarization curve after 360 h of exposure in 3.5 wt.% NaCl solution (Fig. 8.5). The Al^{3+} ions are generated after oxidation of Al whereas OH^- ions are released after oxygen reduction reaction (equation 8.3). The passive region might form from the transformation of $Al(OH)_3$ into Aluminum oxide on the surface during prolong exposure [177].

$$H_2O + \frac{1}{2}O_2 + 2e^- \rightarrow 2OH^- \tag{8.3}$$

$$Al^{+++} + 3OH^- \rightarrow Al(OH)_3 \tag{8.4}$$

$$2Al(OH)_3 \rightarrow Al_2O_3.3H_2O \tag{8.5}$$

$Al(OH)_3$ is insoluble in neutral pH solution and gets accumulated at the interface of metal/solution of the Al alloy and results in formation of corrosion products [178]. During anodic scanning, $Al(OH)_3$ oxidizes into aluminum oxide with increase in potential in another region and subsequently gets accumulated on the alloy which is main reason for the formation of passive region. The different corrosion characteristics of the Al alloy shown after 360 h of exposure in 3.5 wt.% NaCl solution is due to heterogeneous microstructure, impurities, segregation, morphology, distribution of second phase precipitates attributed to surface treatment [179]. In 3.5 wt.%NaCl neutral pH solution, the anodic current in

passive region is almost consistent, low and identical, due to suppressed uniform corrosion by neutral oxide layer (Al_2O_3). The cathodic current density is dependent on size and volume fraction of precipitates which act as local cathode and the volume of oxidant such as dissolved oxygen dominates over the reaction. The solution containing Cl^- ions accelerates the corrosion process of Al alloy by attacking on oxide films. Thus, gradual increment in anodic current is observed after passive region due to attack of Cl^- ions on applied potential which causes dissolution of the aluminum oxide (equation 8.6). This corrosion product (Al_2O_3) has dual nature, the inner layer is adherent, compact and stable whereas the outer layer is porous, less stable and more susceptible to corrosion [180, 181]. The high concentration of Cl^- ions led to breakdown of the oxide film and formed trans-passive region according to following reactions [182, 183]:

$$Al \rightarrow Al^{3+} + 3e^- \tag{8.6}$$

$$Al^{4+} + 4Cl^- \rightarrow AlCl_4^- \tag{8.7}$$

After the trans-passive region, the polarization curve shows limiting current which was due to the deposition of thick corrosion product.

XPS results suggest that a layer of Al_2O_3 is present for the both un-USSP as well as USSP 15 samples as shown by the peak at 74.7 eV (Fig. 8.6 a & 8.6c). The first peak at 74.7 eV of Al_2O_3 has intensity higher than the second at 71.9 eV of Al matrix, this indicates that the oxide layer is thin. The self-passivation for the USSP 15 was highest as the intensity of matrix peak for the USSP 15 was relatively lower as compared to that of the

un-USSP [184]. The increased area of grain boundaries promotes passivation tendency of the oxide layer [185]. There is formation of thicker oxide layer over the surface of the USSP treated specimens due to the presence of nanocrystalline surface layer. After 360 hours of exposure for the USSP 15 specimens no peaks of Al matrix were observed whereas as it was there for the un-USSP, which clearly indicates that the layer formed on the surface of the specimen was more homogeneous. Trdan et. al [161] showed that laser shock peening process transforms the amorphous Al_2O_3 into more stable oxide which resulted in improved corrosion resistance. From the XPS results it can be derived that the protective layer of Al_2O_3 along with $Al(OH)_3$ enhanced the corrosion resistance of the USSP treated specimens.

USSP treatment effectively induces nanocrystalline layer on the surface of the 7075 aluminium alloy. Corrosion current density and corrosion potential of the USSP 15 suggest enhanced corrosion resistance. Severe plastic deformation caused grain refinement and thus increased grain boundaries and dislocation density. The fine-grained layer with more number of grain boundaries reduces the chloride concentration per grain boundary thus resulting in lesser current density [166, 186]. Polycrystalline materials are attacked preferentially during corrosion due to segregation of impurities, imperfect atomic structure and high energy [187]. High density of grain boundaries and dislocations act as sites for passive layer formation and suppress dissolution in the passive state [68–70]. The higher charge transfer resistance of the passive film in the EIS indicates higher stability of the passive film even after prolonged duration of exposure. The refinement/dissolution of the second phase precipitates was also observed after the USSP treatment. Homogeneous

distribution of refined precipitates throughout the matrix promotes formation of adherent and uniform passive layer. It has been reported that passive film may be different in stability or may even be absent on second phase in aluminium alloys [188]. For ultrafine grained Fe-Cr alloy higher concentration of Cr was reported at the surface than in the coarse-grained counterpart and this enrichment of Cr at the surface resulted in higher passivation [189]. Therefore, for USSP treated sample a more stable and uniform passive film was formed on the surface causing more positive corrosion potential and smaller current density.

Plastic deformation imparts residual stress near the surface region which is mostly compressive in nature. The extent and intensity of compressive residual stress depends on the USSP treatment parameters. Takakuwa et al. [190] reported that reduction of inter atomic spacing enables growth of passive layer due to compressive stress. The corrosion current density decreased with increase in compressive stress and this improved corrosion resistance. In the present study also the induced compressive stress resulting from USSP treatment would have facilitated the formation of passive layer over the surface of the USSP 15 specimen. Krawiec et al. [75] found increment in charge transfer and oxide film resistance after aging in air, due to the compressive residual stresses resulting from laser shock peening (LSP) treatment which resulted in enhancement in electrochemical behavior of AA2050-T8. Trdan et al. [191] studied the effect of LSP on corrosion behavior of AA6082-T65 in 3.5% NaCl solution and found that LSP improves corrosion resistance, reduces surface pitting and intergranular attacks. This could be attributed to the low surface roughness in LSP in comparison to SP, as well as higher induced compressive

residual stresses.

The plastic deformation resulting from USSP treatment induced high density of dislocations near the surface region of the alloy. It has been reported that increase in dislocation density provides active sites for corrosion [192]. With increase in USSP duration the extent of deformation increases which also results in increment in dislocation density. Increase in the size of balls and treatment duration of SMAT increases the extent of deformation which reduced the corrosion rate of 409SS [77]. Increase in corrosion rate for the samples treated beyond the duration of 15 seconds may be attributed to increase in dislocation density and the surface defects. Although for some cases increase in dislocation density results in increase of corrosion resistance. Huang et al. [193] reported improvement in passivation behavior of Ti–25Nb–3Mo–3Zr–2Sn alloy post SMAT and attributed to high density of dislocations. Once a passive layer is formed, it acts as a barrier and results in improvement of corrosion resistance. The stability of the passive film is dependent on the interfacial bonding between the substrate and the film. The poor polarization resistance of the sandblast-annealed Ti was due to poor interfacial bonding between the passive film and the substrate resulting from high density of dislocation near the surface region [146]. Hence, it may be the increase in dislocation density which resulted in deterioration of corrosion resistance of the samples USSP treated for longer duration.

From the stress corrosion sensitivity coefficient it is clear that USSP treatment significantly enhanced the SCC resistance of the AA7075 in 3.5 wt.% NaCl solution. Fig. 8.11 shows the fracture surfaces of AA7075 alloy after SSRT in air and 3.5 wt% NaCl solution in un-USSP and USSP condition respectively. It is evident from lower value of the stress

corrosion sensitivity coefficient of the USSP treated sample (13.2%) that its resistance against the SCC in 3.5 wt% NaCl solution is significantly enhanced. The fracture characteristics of the un-USSP and USSPed samples under SSRT in air and 3.5 wt% NaCl solution were examined. The fracture surfaces of the un-USSPed specimens tested under SSRT in air and 3.5 wt% NaCl solution are shown by SEM micrographs in Fig. 8.11(a&b) respectively. It may be seen that there is large number of dimples and a few flat regions on fracture surface of the un-USSPed samples tested in air (Fig. 8.11a), whereas the number of dimples on fracture surface of the un-USSPed samples tested in 3.5 wt% NaCl solution is drastically reduced and there is significant increase in faceted fracture (Fig. 8.11b). More or less there is similar effect of SSRT of the USSPed specimens tested in air and 3.5 wt% NaCl solution like that of the un-USSP in the corresponding environments. Likewise the time to failure of the un-USSP and USSPed specimen under SSRT in air was almost comparable, whereas the time to failue of the USSPed specimens in the 3.5 wt% NaCl solution was appreciably higher with respect to that of the un-USSP treated in 3.5 wt% NaCl solution (Fig. 8.8).

Fig. 8.12 shows the longitudinal section of the un-USSP and USSP samples exposed to 3.5 wt.% NaCl solution and it is clear that pitting caused by the highly rigorous environment led to formation of cracks from the surface during loading. During the crack initiation stage, there would be more grains to bear the crack driving force in the fine grain region so that the stress concentration is reduced and the crack initiation is delayed. During the crack propagation stage, more grain boundaries in the fine grain region would

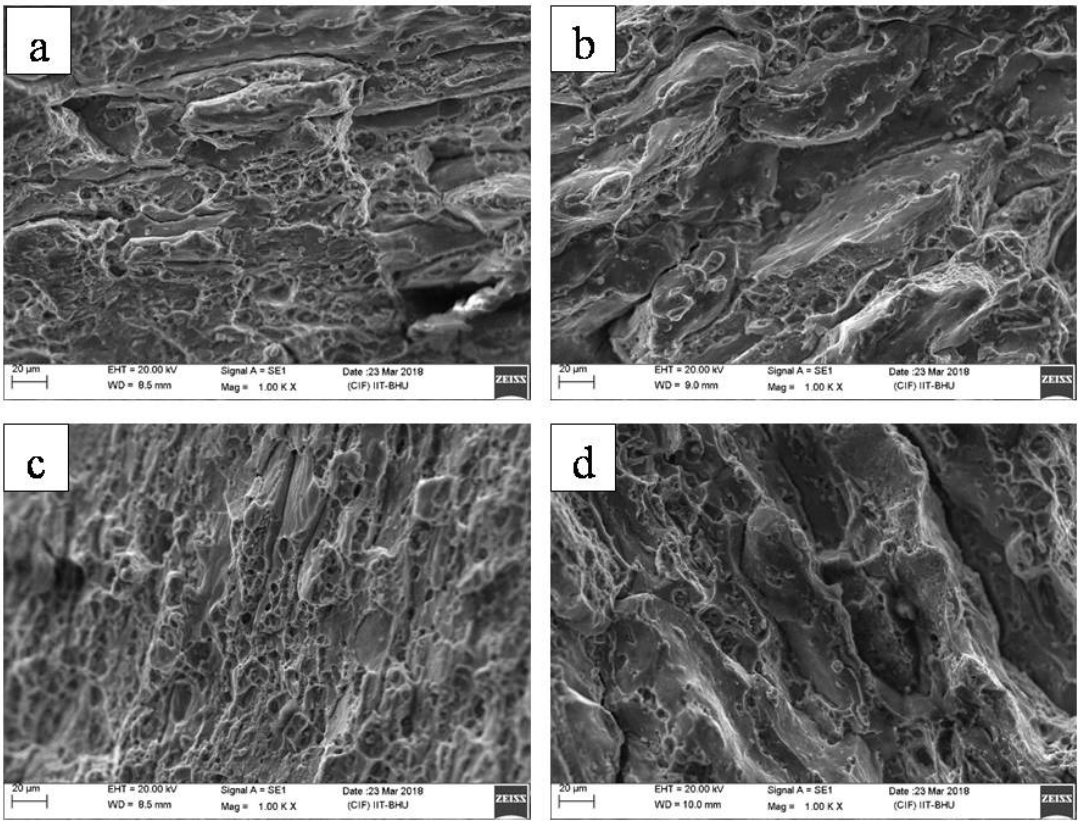

FIGURE 8.11: Fracture surfaces of the SSRT samples in un-USSP condition tested in (a) air, (b) 3.5 wt% NaCl solution and in USSP condition tested in (c) air and (d) 3.5 wt% NaCl solution.

increase the resistance for the micro-crack propagation along or across the grain boundaries. In this way, the tiny nanometer grain would reduce the crack propagation rate and make the stress corrosion sensitivity coefficient decline [194]. Sano et. al [195] reported that compressive residual stress plays a significant role in stress corrosion cracking resistance, it counteracts the part of tensile stress and delays fracture. So the increase in the stress corrosion resistance from the USSP treated specimen can mainly be attributed to the grain refinement introduced during the high energy peening and the high level of compressive residual stresses.

Significant improvement in corrosion and stress corrosion resistance for the USSP

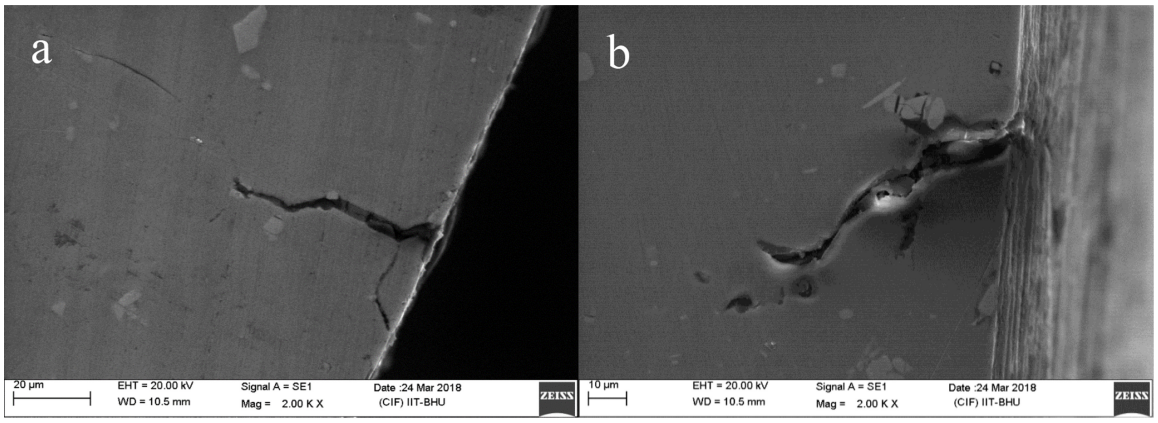

FIGURE 8.12: SEM micrograph of longitudinal section of SSRT tested samples in 3.5 wt.% NaCl (a) un-USSP and (b) USSP conditions.

15 sample is thus due to ultrafine grain size and reduction in the size of the second phase precipitates in combination with high dislocation density and lower surface roughness. These parameters in combination led to formation of adherent passive layer which ultimately enhanced the corrosion resistance of the 7075 aluminium alloy.

8.6 Conclusions

The following conclusions are drawn from this chapter:

1. Potentiodynamic polarization showed improved ability for passivation with a decrease in corrosion current density after the USSP treatment. Electrochemical impedance spectroscopy revealed that polarization resistance R_p increased significantly and double layer capacitance (C_{dl}) was found to be decreased after the USSP treatment indicating lower corrosion activity on the metal solution interface, compared to that of the un-USSP.

2. After prolonged immersion of 360 hours in 3.5 wt.% NaCl, the USSP 15 sample exhibited superior corrosion resistance which confirms that this surface treatment is effective even for longer service duration.

3. The SEM/EDS results confirmed that pitting was probably associated with the cathodic second phase precipitates. Based on schematic it was proposed that due to lower galvanic coupling between the matrix and precipitates the USSP treated sample exhibited lower pitting tendency and also benefited in passive layer formation. The passive layer mainly constituted of $Al(OH)_3$ along with Al_2O_3 which was confirmed by XPS analysis.

4. All the samples USSP treated for different durations showed enhanced corrosion resistance as compared to that of the un-USSP but the sample USSP treated for 15 seconds showed the best corrosion resistance amongst the all even after prolonged immersion in aggressive environment.

5. The enhanced stress corrosion resistance of the USSP treated sample is mainly due to the combined effect of compressive residual stress and nanostructured surface layer.